
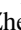







Field-induced valence fluctuations in YbB₁₂R. Kurihara ¹, A. Miyake,¹ M. Tokunaga ¹, A. Ikeda ¹, Y. H. Matsuda,¹ A. Miyata,² D. I. Gorbunov,² T. Nomura ^{1,2}, S. Zherlitsyn ², J. Wosnitzer,^{2,3} and F. Iga ⁴¹*Institute for Solid State Physics, The University of Tokyo, Kashiwa, Chiba 277-8581, Japan*²*Hochfeld-Magnetlabor Dresden (HLD-EMFL) and Würzburg-Dresden Cluster of Excellence ct.qmat, Helmholtz-Zentrum Dresden-Rossendorf, 01328 Dresden, Germany*³*Institut für Festkörper- und Materialphysik, Technische Universität Dresden, 01062 Dresden, Germany*⁴*Institute for Quantum Beam Sciences, Ibaraki University, Mito 310-8512, Japan* (Received 19 October 2020; revised 31 January 2021; accepted 16 February 2021; published 3 March 2021)

We performed high-magnetic-field ultrasonic experiments on YbB₁₂ up to 59 T to investigate the valence fluctuations in Yb ions. In zero field, the longitudinal elastic constant C_{11} , the transverse elastic constants C_{44} and $(C_{11} - C_{12})/2$, and the bulk modulus C_B show a hardening with a change of curvature at around 35 K indicating a small contribution of valence fluctuations to the elastic constants. When high magnetic fields are applied at low temperatures, C_B exhibits a softening above a field-induced insulator-metal transition signaling field-induced valence fluctuations. Furthermore, at elevated temperatures, the field-induced softening of C_B takes place at even lower fields and C_B decreases continuously with field. Our analysis using the multipole susceptibility based on a two-band model reveals that the softening of C_B originates from the enhancement of multipole-strain interaction in addition to the decrease of the insulator energy gap. This analysis indicates that field-induced valence fluctuations of Yb cause the instability of the bulk modulus C_B .

DOI: [10.1103/PhysRevB.103.115103](https://doi.org/10.1103/PhysRevB.103.115103)**I. INTRODUCTION**

Since the electronic and magnetic properties of materials are mainly determined by valence electrons, a precise knowledge about the valence state is important in material science. Especially for $4f$ -electron systems, the valence determines the total angular momentum J , the localized (or delocalized) $4f$ -electron character, and corresponding wave functions. A noninteger valence state appears in some rare-earth compounds with Ce, Sm, Eu, and Yb ions. In such materials, valence fluctuations due to hybridization between conduction electrons and $4f$ electrons play a key role in their physical properties. YbB₁₂ is one of the valence fluctuating materials with such a c - f hybridization, a high-Kondo temperature, and insulating character [1,2].

YbB₁₂ has the UB₁₂-type crystal structure belonging to the $Fm\bar{3}m$ (O_h^5) space group [1]. The Γ_8 ground state of the $4f$ electrons based on Yb³⁺ configuration in the crystal electric field (CEF) has been proposed [3,4]. The almost degenerated Γ_7 and the Γ_6 states at 270 K (23 meV) were considered as excited states [3,4]. These CEF states based on the $J = 7/2$ can be consistent with the hyperfine coupling constant for free Yb³⁺ ions determined by NMR measurements [5]. In contrast, a nonmagnetic ground state has been suggested from the temperature-independent magnetic susceptibility at low temperatures [6,7]. Indication for a strongly hybridized electronic state was found using bulk-sensitive x-ray photoelectron spectroscopy showing a slight deviation from the valence Yb³⁺ [8]. The hybridization between $5d$ conduction electrons and $4f$ localized electrons has been proposed as

a candidate mechanism for an observed band-gap opening [9,10]. The contribution of the B- $2p$ electrons to the c - f hybridization is also discussed as a result of $dd\sigma$ hopping through B₁₂ clusters.

In addition to the CEF scheme, several characteristic energies related to the insulating character have been studied in YbB₁₂. Both in a polycrystal and single crystal, resistivity measurements show evidence for two activation energies of ~ 30 and 65 K [6,7]. A density of states with two-double peaks was proposed as a mechanism of two activation energies [11]. NMR and specific-heat data have been described by a simple two-band model, each band having a bandwidth of 55 K, and with an energy gap of 140 K at the Fermi energy [6,12]. High-resolution photoemission spectroscopy suggested a hybridization gap of 170 K (15 meV) below 150 K and strongly hybridized character below 60 K [13].

In YbB₁₂, various high-magnetic-field studies were performed to elucidate the mechanism of the formation of the energy gap. High-field magnetoresistance measurements indicated that the energy gap of 30 K closes around 45 T while the other gap remains up to higher fields [11]. Magnetization measurements revealed metamagnetic behavior at insulator-metal (IM) transitions at $B_{IM} = 47$ T for $B||[001]$ and 54 T for $B||[110]$ and $B||[111]$ [14]. Another magnetization anomaly indicating the saturation of magnetization appears at 102 T [15]. The energy shift of the $4f$ band due to the Zeeman effect was proposed to explain the closing of the band gap of 170 K. Synchrotron x-ray absorption spectra showed the field independence of the L_3 edge indicating no considerable change of the Yb valence in the field-induced metal phase

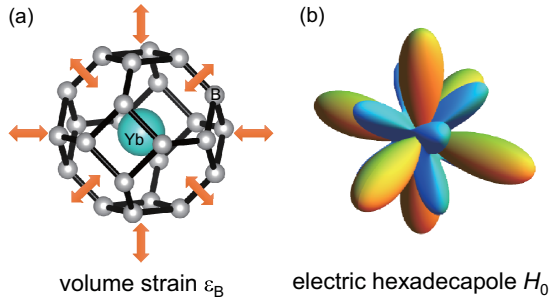


FIG. 1. Schematic view of the volume strain and the hexadecapole in YbB_{12} . (a) Crystal lattice around the Yb ion [4] and volume strain ε_B with the irrep Γ_1 of O_h . Orange arrows indicate the isotropic deformation of the lattice. (b) Hexadecapole H_0 with Γ_1 symmetry obtained as a result of an isotropic change of the Yb ionic radius.

[16]. Specific-heat measurements revealed a discontinuous enhanced of Sommerfeld coefficient $\gamma \sim 60$ mJ/mol K², and a corresponding Kondo temperature of 220–250 K above the IM transition, suggesting that the high-field phase is a valence-fluctuating Kondo metal [17]. These high-field experiments indicate a contribution of the c - f hybridization to the opening of the energy gap in YbB_{12} . Magnetic quantum oscillations in the insulating phase have also been focused to understand the insulating character of YbB_{12} [18].

To further investigate the valence fluctuations caused by the c - f hybridization in YbB_{12} , we focused on ultrasonic measurement. Since a valence change causes an isotropic change of the ionic radii, an isotropic volume change of the crystal lattice is induced and the CEF Hamiltonian H_{CEF} of Eq. (B1) (see Appendix B) is changed to $H_{\text{CEF}} + (\partial H_{\text{CEF}}/\partial \varepsilon_B)\varepsilon_B$. Here ε_B is the volume strain with the irreducible representation (irrep) Γ_1 of the O_h symmetry. This additional term to the CEF is described as a coupling between ε_B and a hexadecapole H_0 with Γ_1 in YbB_{12} . The schematic view of ε_B and H_0 in YbB_{12} are shown in Figs. 1(a) and 1(b), respectively. Based on simple Landau theory for elasticity, the total free energy consists of a lattice and an electronic part is given by [19]

$$F = \frac{1}{2}C_B^0\varepsilon_B^2 + \frac{1}{2}\alpha H_0^2 - g_B H_0 \varepsilon_B. \quad (1)$$

Here g_B is the coupling constant between the strain and H_0 , C_B^0 is the bulk modulus without multipole contribution, and α is a coefficient. The first and second terms on the right-hand side of Eq. (1) correspond to the energy loss due to the deformation of the lattice and the increase of the hexadecapole moment,

respectively. The third term corresponds to the energy gain of the electronic state due to the hexadecapole-volume strain interaction. The response of the hexadecapole appears as a result of the decrease in the bulk modulus as $C_B^0 - g_B^2/\alpha$.

As shown in previous reports [20–22], ultrasonic measurements are a powerful tool to detect valence fluctuations. In particular, in the Kondo insulator SmB_6 , the decrease in the bulk modulus C_B with decreasing temperatures, namely the elastic softening of C_B , has been revealed as a result of valence fluctuations between Sm^{2+} and Sm^{3+} [23]. The relation between the energy gap of c - f hybridized bands and the elastic softening is also discussed in terms of the interaction between $4f$ electrons and the bulk strain ε_B with full symmetry Γ_1 . Several theoretical studies have proposed such a contribution of the c - f hybridization to the elasticity [24–27]. Therefore, we measured relevant elastic constants in zero and high fields searching for an elastic softening related to the valence fluctuations in YbB_{12} .

This paper is organized as follows. In Sec. II experimental details of sample preparation and ultrasonic measurements in pulsed magnetic fields are explained. In Sec. III we present the results of our ultrasonic experiments of YbB_{12} . In zero field an increase in the elastic constants with decreasing temperatures, namely elastic hardening, accompanying curvature changes reveals some contribution of valence fluctuations to the elasticity. In contrast to zero field, a field-induced softening of the bulk modulus C_B appears, which indicates field-induced valence fluctuations due to c - f hybridization. In Sec. IV we analyzed the measured elastic constants using a multipole-susceptibility model. The field-induced valence fluctuations can be described in terms of the hexadecapole-volume strain coupling. Our analysis also confirms the decrease of the energy gap in high fields. We summarize our results in Sec. V.

II. EXPERIMENT

Single crystals of YbB_{12} were grown using the floating-zone method [7]. Laue x-ray backscattering was used to align, cut, and polish samples with (110), ($\bar{1}\bar{1}0$), ($\bar{1}10$), ($\bar{1}\bar{1}0$), (001), and (00 $\bar{1}$) faces and the size of $1.033 \times 1.030 \times 3.763$ mm³. An ultrasound pulse-echo method with a numerical vector-type phase-detection technique was used to measure the ultrasound velocity v [28]. The elastic constant $C = \rho v^2$ was determined from v and the calculated mass density $\rho = 4.828$ g/cm³ using the lattice constant $a = 7.469$ Å [1]. Piezoelectric transducers using LiNbO_3 plates with a 36° Y-cut and 41° X-cut (Yamaju Ceramics Co.) were employed to generate

TABLE I. Symmetry strains, electric multipoles, and elastic constants corresponding to the irreducible representations (irreps) of the space group O_h .

Irrep	Symmetry strain	Electric multipole	Elastic constant
Γ_1	$\varepsilon_B = \varepsilon_{xx} + \varepsilon_{yy} + \varepsilon_{zz}$	$O_4^0 + 5O_4^4 (= H_0)$	$C_B = (C_{11} + 2C_{12})/3$
Γ_3	$\varepsilon_u = (2\varepsilon_{zz} - \varepsilon_{xx} - \varepsilon_{yy})/\sqrt{3}$	$O_{u(=3z^2-r^2)}$	$C_T = (C_{11} - C_{12})/2$
	$\varepsilon_v = \varepsilon_{xx} - \varepsilon_{yy}$	$O_{v(=x^2-y^2)}$	
Γ_5	ε_{yz}	O_{yz}	C_{44}
	ε_{zx}	O_{zx}	
	ε_{xy}	O_{xy}	

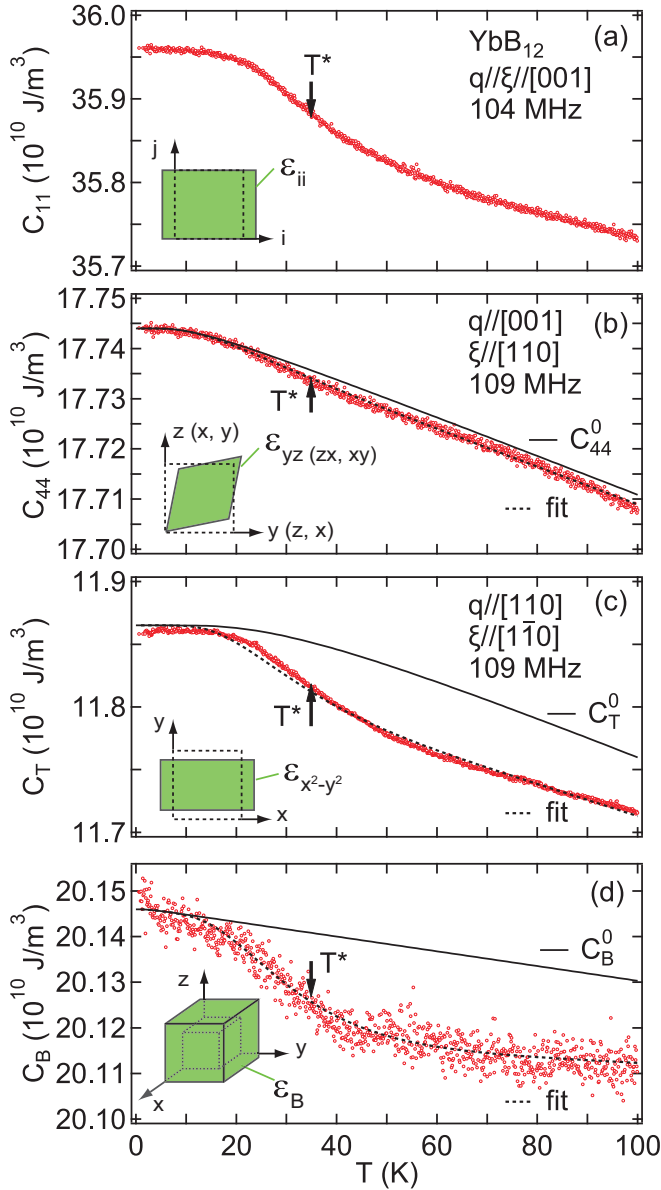


FIG. 2. Temperature dependence of (a) the longitudinal elastic constant C_{11} , the transverse elastic constants (b) C_{44} and (c) $C_T = (C_{11} - C_{12})/2$, and (d) the bulk modulus C_B calculated from C_{11} and C_T . The dotted lines indicate the fit of C_{44} , C_T , and C_B in the framework of the phenomenological two-band model discussed in Sec. IV. The solid lines indicate the temperature dependence of the elastic constants without multipole contribution. The strains ε_{ij} for C_{11} , C_{44} , C_T , and C_B are schematically shown in the inset in each panel. The vertical arrows in each panel indicate the characteristic temperature T^* discussed in Sec. IV.

longitudinal ultrasonic waves with the fundamental frequency of approximately $f = 30$ MHz and transverse waves with 18 MHz, respectively. As indicated in Fig. 2, higher-harmonic frequencies were used to obtain high-resolution data. A room temperature vulcanizing rubber (Shin-Etsu Silicone KE-42T) was used to glue the LiNbO_3 onto the sample. The direction of ultrasonic propagation q and the direction of polarization ξ for the elastic constant C_{ij} are indicated in Fig. 2. Two nondestructive pulsed magnets were used: one with a pulse duration

of 36 ms installed at the Institute for Solid State Physics, the University of Tokyo using a ^4He cryostat, and another magnet with a pulse duration of 150 ms at the HLD-EMFL in Dresden using a ^3He cryostat.

III. RESULTS

A. Temperature dependence of elastic constants

To gain more information on the Yb valence in YbB_{12} , we investigated the three elastic constants C_{11} , C_{44} , and $C_T = (C_{11} - C_{12})/2$. Their relations to the symmetry strain and electric multipole are summarized in Table I [19,29]. Figure 2 shows the temperature dependence of the elastic constants in zero field. We observed the elastic hardening of C_{11} , C_{44} , and C_T with lowering temperatures. We also observed the elastic hardening of C_{11} from 300 K (see Appendix A). All elastic constants exhibit an additional hardening and a characteristic curvature change in the vicinity of $T^* = 35$ K. As shown by the solid curves in Fig. 2, the elastic constants would exhibit a monotonic increase with decreasing temperature [30] if we do not consider multipole contributions, described in the following Sec. IV [19]. Therefore, the additional features in the elastic constants of YbB_{12} indicate the multipole contribution to elasticity.

To describe the origin of the anomaly in each elastic constant of YbB_{12} , we focus on the multipole effect of the CEF wave functions of localized $4f$ electrons taken into account the presence of Γ_8 , Γ_7 , and Γ_6 states [3,4]. Since the direct product of the Γ_8 quartet is reduced as $\Gamma_8 \otimes \Gamma_8 = \Gamma_1 \oplus \Gamma_2 \oplus \Gamma_3 \oplus 2\Gamma_4 \oplus 2\Gamma_5$ [29,31], we deduce that the Γ_8 ground-state wave functions carry the electric quadrupoles O_u and O_v with irrep Γ_3 and O_{yz} , O_{zx} , and O_{xy} with irrep Γ_5 as summarized in Table I. In addition, the Γ_8 quartet also provides the electric hexadecapole $H_0 = O_4^0 + 5O_4^4$ with irrep Γ_1 . Because the magnetic multipole degrees of freedom do not couple with the strain, we ignore magnetic dipoles with irrep Γ_4 and magnetic octupoles with irreps Γ_2 , Γ_4 , and Γ_5 . This group-theoretical consideration indicates that the elastic softening of $(C_{11} - C_{12})/2$ with irrep Γ_3 and C_{44} with irrep Γ_5 is due to a multipole-strain interaction described as

$$H_{\text{MS}} = -g_{\Gamma_\gamma} O_{\Gamma_\gamma} \varepsilon_{\Gamma_\gamma}. \quad (2)$$

Here g_{Γ_γ} is a coupling constant and Γ_γ denotes the irrep. We show how to calculate the multipole susceptibility based on the CEF wave functions in Appendix B. Because the calculated multipole susceptibility for Γ_3 - and Γ_5 -type quadrupoles shows a divergent increase for decreasing temperatures, a divergent elastic softening is theoretically expected in C_{44} and C_T . However, our experimental results show no softening in all measured elastic constants. Therefore, the CEF approach based on a localized $4f$ character does not apply to the elasticity of YbB_{12} in zero field.

The other possible scenario describing the additional contribution around T^* is a result of the charge freezing of Yb without long-range ordering as previously discussed in the samarium compounds Sm_3Se_4 and Sm_3Te_4 [20,21]. Since the charge freezing would be characterized by a frequency-dependent ultrasonic response, we measured the elastic constants and ultrasonic attenuation coefficients for several frequencies. However, we did not observe any frequency

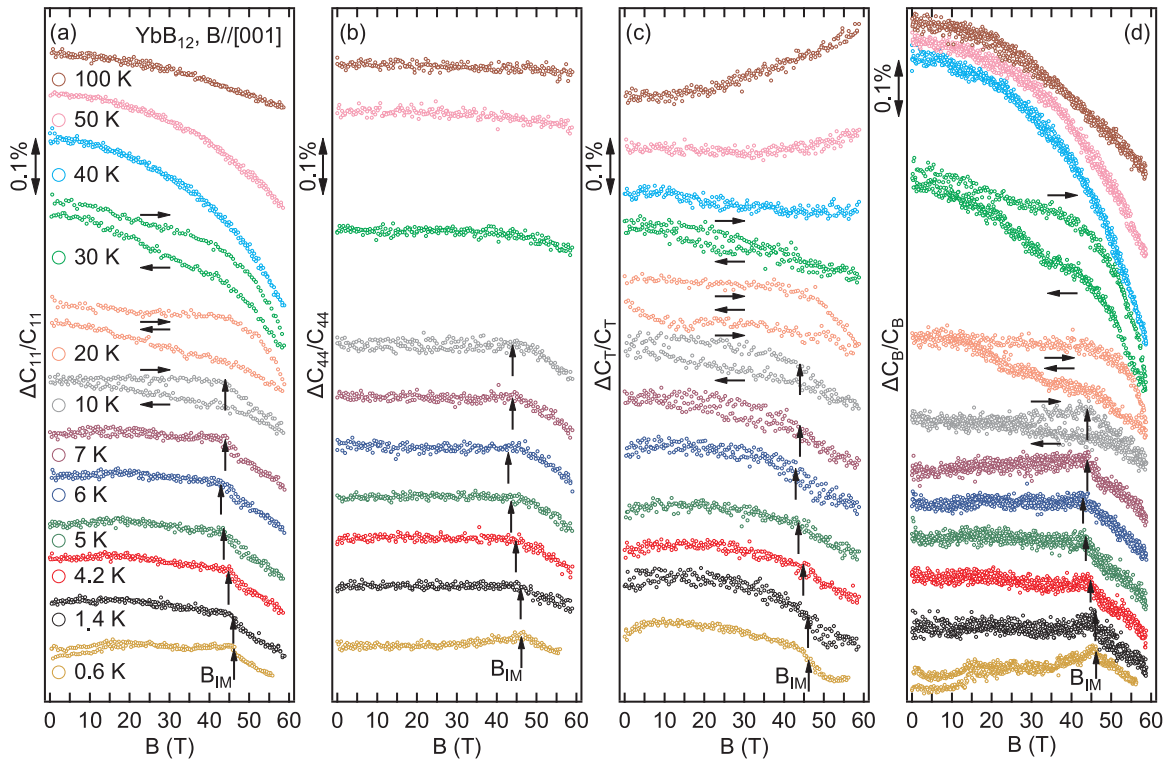


FIG. 3. Magnetic-field dependence of the relative variation of the elastic constants $\Delta C_{ij}/C_{ij} = [C_{ij}(B) - C_{ij}(B=0)]/C_{ij}(B=0)$ at several temperatures for $B||[001]$. Field dependence of (a) the longitudinal elastic constant C_{11} , the transverse elastic constants (b) C_{44} and (c) C_T , and (d) the bulk modulus C_B . The data sets are shifted consecutively along the $\Delta C/C$ axes for clarity. The vertical arrows indicate the insulator-metal transition field B_{IM} . The horizontal arrows show the field-sweep directions.

dependence neither in the elastic constants nor in the ultrasonic attenuation coefficients between 30 and 160 MHz.

Therefore, we focus on the contribution of valence fluctuations to the elasticity caused by the c - f hybridization. Figure 2(d) shows the temperature dependence of the bulk modulus $C_B = (C_{11} + 2C_{12})/3 = C_{11} - 4C_T/3$ with the irrep Γ_1 calculated from the experimental results of C_{11} and C_T . C_B exhibits as well a hardening with an additional contribution in the vicinity of 35 K. This result for YbB_{12} is in contrast to the significant softening of C_B due to Sm valence fluctuations observed in SmB_6 . In Sec. IV we will discuss the origin of the additional contribution in terms of the multipole susceptibility based on a two-band model to confirm the contribution of valence fluctuations to the elastic constants in zero field.

B. Magnetic-field dependence of elastic constants

To investigate the valence properties of YbB_{12} in magnetic fields, we measured the elastic constants C_{11} , C_{44} , and C_T up to 59 T for $B||[001]$. Figure 3 shows the magnetic-field dependence of the relative variation of the elastic constants $\Delta C_{ij}/C_{ij}$ at several temperatures. We observed a field-induced IM transition and elastic softening for each elastic constant in the Kondo-metal phase. Below 10 K, this softening appears rather abruptly above the insulator-metal transition field B_{IM} . B_{IM} are comparable with results of a previous magnetocaloric-effect study [17]. Since C_B contains C_{11} and C_T , our experimental results show as well the softening of C_B in the Kondo-metal phase.

Above 10 K, no sharp anomaly corresponding to the Kondo-metal phase transition is visible any more. However, C_{11} still shows a significant softening in magnetic field contrary to the other elastic constants (Fig. 3). In particular, at 40 K, C_{11} exhibits a large softening of 0.30% at 59 T while C_T shows a softening of only 0.027%. The softening of C_{11} at 100 K is also in contrast to the hardening observed for C_T .

Between 10 and 30 K a clear hysteresis appears in the pulsed-field data of C_{11} and C_T (Fig. 3). This is approximately the temperature range where the additional contribution to the elastic constants is detected (Fig. 2). As shown in a previous magnetocaloric-effect study in adiabatic condition below 7 K [17], the temperature of the sample is reduced by the application of a magnetic field. Because of the quasiadiabatic experimental conditions, the final temperature after the field pulse might be higher than assumed which may cause the hysteresis. Therefore, the hysteresis of elastic constants C_{11} and C_T can also be attributed to the magnetocaloric effect.

We also looked for the quantum oscillation in YbB_{12} [18]. In principle, such quantum oscillations may appear as well in bulk sensitive ultrasound properties. However, we were not able to resolve any acoustic de Haas-van Alphen effect at least 0.6 K. This result may imply a weak electron-phonon interaction for the studied acoustic modes.

We calculated $C_B = C_{11} - 4C_T/3$ from the measured magnetic-field dependence of C_{11} and C_T (Fig. 3). Indeed, C_B shows a very similar behavior as the individual elastic constants with a clear anomaly at B_{IM} below 10 K and

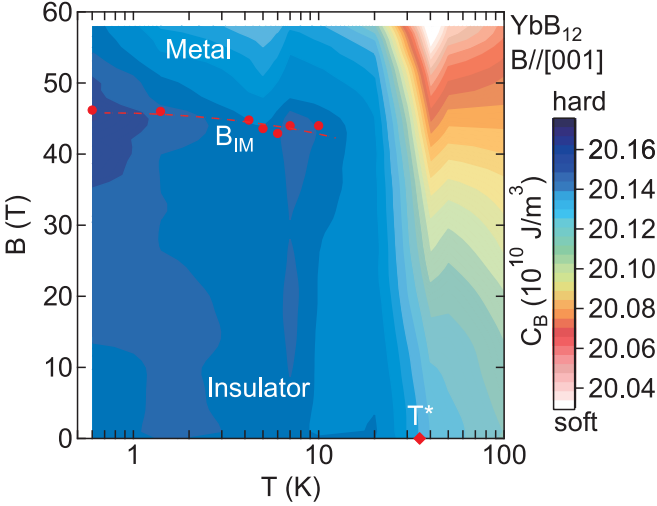


FIG. 4. Temperature-field phase diagram of YbB_{12} for $B\parallel[001]$. The filled red circles indicate the insulator-metal transition field B_{IM} . The filled red diamond indicates the characteristic temperature T^* (see text for details). The color code shows the value of the bulk modulus C_B (field up-sweep).

hysteresis between 10 and 30 K. B_{IM} determined by our ultrasonic measurements are shown in Fig. 4.

C_B exhibits a small softening below 50 T at 20 K and 45 T at 30 K. By contrast, above 40 K, C_B shows monotonic softening with increasing fields. In particular, the largest softening of 0.52% is observed in C_B at 40 K. The field-induced elastic softening of C_B is summarized in the contour plot in Fig. 4.

For further understanding of the field-induced elastic softening in YbB_{12} , we plotted the temperature dependence of C_B for various magnetic fields (Fig. 5). As shown in the inset of

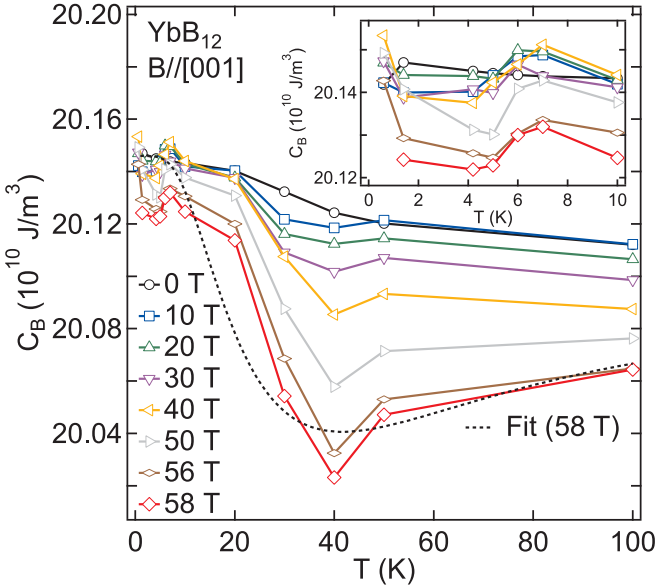


FIG. 5. Temperature dependence of the bulk modulus C_B of YbB_{12} at various magnetic fields for $B\parallel[001]$ extracted from the up-sweep data shown in Fig. 3, except for the zero-field data. The dotted line indicates the fit describing C_B in the framework of the phenomenological two-band model. The inset shows C_B below 10 K.

Fig. 5, C_B exhibits a softening of about 0.05% below 7 K down to ~ 2 K in magnetic fields above 40 T. In addition, C_B shows significant softening from 100 K down to 40 K in high fields, which is in contrast to the hardening of C_B in zero field. The softening of C_B is similar to that found for SmB_6 caused by c - f hybridization-driven valence fluctuations corresponding to hexadecapole-strain interaction [23].

The experimental results of the temperature dependence and the magnetic field dependence of C_B of YbB_{12} cannot be described by the localized $4f$ -electron model (see Appendix C). In the following Sec. IV, therefore, we discuss our observations in terms of multipole-strain interaction and the multipole susceptibility for a two-band model.

IV. DISCUSSION

We discuss the origin of the elastic anomalies of YbB_{12} in terms of a two-band model assuming a constant density of states (DOS) with respect to energy. This model has successfully reproduced the elastic softening observed in the Kondo compounds SmB_6 and CeNiSn [23,32]. In YbB_{12} , this phenomenological model also gives qualitative explanation for the temperature dependence of C_{44} , C_T , and C_B in zero field and for C_B in high fields. Field-induced valence fluctuations are included by the hexadecapole-strain interaction. By that, the essential parameters for the explanation of our experimental results are identified (Table II).

We introduce a two-band model, which is schematically shown in Fig. 6. In this model we deal with the two c - f hybridized bands: an upper band above the Fermi energy E_F with an energy $E_{0,k}^u$ and a lower band below E_F with $E_{0,k}^l$. The DOS with energy dispersion of each band is simplified to the rectangular form. The bandwidth W , the DOS D , and the band gap 2Δ are set as shown in Fig. 6. We assume that the multipole-strain interaction for the electrons in the two bands can be written as [33]

$$H_{\text{MS}} = - \sum_{\mathbf{k}} \begin{pmatrix} c_{\mathbf{k},u}^\dagger \\ c_{\mathbf{k},l}^\dagger \end{pmatrix}^T \begin{pmatrix} d_{\mathbf{k},\Gamma_\gamma}^u & h_{\mathbf{k},\Gamma_\gamma} \\ h_{\mathbf{k},\Gamma_\gamma}^* & d_{\mathbf{k},\Gamma_\gamma}^l \end{pmatrix} \begin{pmatrix} c_{\mathbf{k},u} \\ c_{\mathbf{k},l} \end{pmatrix} \varepsilon_{\Gamma_\gamma}. \quad (3)$$

For the multipole-strain interaction H_{MS} of Eq. (2), the diagonal term $d_{\mathbf{k},\Gamma_\gamma}^{l(u)}$ for the electrons in band $u(l)$ indicates a renormalized multipole-strain coupling constant described as $g_{\Gamma_\gamma} \langle u(l) | O_{\Gamma_\gamma} | u(l) \rangle$. The off-diagonal term $h_{\mathbf{k},\Gamma_\gamma}$ is written as $g_{\Gamma_\gamma} \langle u(l) | O_{\Gamma_\gamma} | l(u) \rangle$. $c_{\mathbf{k},u(l)}$ and $c_{\mathbf{k},u(l)}^\dagger$ are annihilation and creation operators of an electron in the band $u(l)$ with wave vector \mathbf{k} , respectively. Considering the Anderson Hamiltonian describing c - f hybridization, we deduce that the multipole-strain interaction of Eq. (3) originates from electron-phonon interaction consisting of c - f and f - f terms [27]. The multipole-strain interaction of Eq. (3) for the two-band model provides a second-order perturbation for the upper band, the lower one, and the band gap. The perturbation energies of each band and the perturbation energy gap are described as [23,32]

$$E_{\mathbf{k}}^u(\varepsilon_{\Gamma_\gamma}) = E_{0,\mathbf{k}}^u - d_{\mathbf{k},\Gamma_\gamma}^u \varepsilon_{\Gamma_\gamma} + \frac{|h_{\mathbf{k},\Gamma_\gamma}|^2}{2\Delta_{\mathbf{k}}} \varepsilon_{\Gamma_\gamma}^2, \quad (4)$$

$$E_{\mathbf{k}}^l(\varepsilon_{\Gamma_\gamma}) = E_{0,\mathbf{k}}^l - d_{\mathbf{k},\Gamma_\gamma}^l \varepsilon_{\Gamma_\gamma} - \frac{|h_{\mathbf{k},\Gamma_\gamma}|^2}{2\Delta_{\mathbf{k}}} \varepsilon_{\Gamma_\gamma}^2, \quad (5)$$

TABLE II. Fit parameters determined by the analysis of the elastic constants C_{44} , C_T , and C_B in zero field using the multipole susceptibility given in Eq. (9). Parameters describing C_B at 58 T are also listed. $D = 2.25 \times 10^{27} \text{ K}^{-1} \text{ m}^{-3}$ in zero field is calculated from $|d_B^u - d_B^l|/k_B$. $|d_B^u - d_B^l|/k_B$ of C_B at 58 T is derived from the rigid-band approximation. The parameters for SmB_6 are reproduced from Ref. [23].

C_{Γ_γ}	Δ (K)	W (K)	$D(d_{\Gamma_\gamma}^u - d_{\Gamma_\gamma}^l)^2 (10^9 \text{ J/m}^3)$	$A (10^{10} \text{ J/m}^3)$	$B (\text{J/m}^3)$	C (K)	$ d_{\Gamma_\gamma}^u - d_{\Gamma_\gamma}^l /k_B$ (K)
C_{44}	70	55	0.352	17.744	1.25×10^8	32	106
C_T	70	55	8.58	11.865	1.41×10^9	85	526
C_B (0 T)	70	55	3.30	20.146	9.7×10^6	6	326
C_B (58 T)	37	55	10.3	20.146	9.7×10^6	6	(576)
C_B (SmB_6)	160	150	25.6				1280

$$\Delta_k(\varepsilon_{\Gamma_\gamma}) = \Delta_k - \frac{1}{2}(d_{k,\Gamma_\gamma}^u - d_{k,\Gamma_\gamma}^l)\varepsilon_{\Gamma_\gamma} + \frac{|h_{k,\Gamma_\gamma}|^2}{2\Delta_k}\varepsilon_{\Gamma_\gamma}^2. \quad (6)$$

Here $2\Delta_k = E_{0,k}^u - E_{0,k}^l$ is the energy gap between the upper band and the lower one. The total free energy F is written as [34]

$$F = \frac{1}{2}C_{\Gamma_\gamma}^0 \varepsilon_{\Gamma_\gamma}^2 + nE_F(\varepsilon_{\Gamma_\gamma}) - k_B T \sum_{s=(u,l),k} \ln \left\{ 1 + \exp \left[-\frac{E_k^s(\varepsilon_{\Gamma_\gamma}) - E_F(\varepsilon_{\Gamma_\gamma})}{k_B T} \right] \right\}. \quad (7)$$

Here $C_{\Gamma_\gamma}^0$ is the elastic constant due to the phonon part with the irrep Γ_γ , n is the total number of conduction electrons, $E_F(\varepsilon_{\Gamma_\gamma})$ is the Fermi energy in the deformed system, and k_B is the Boltzmann constant. The first term on the right-hand side of Eq. (7) corresponds to the lattice part. The second and third terms correspond to the free energy of the conduction electrons. The second derivative of the total free energy with respect to the strain $\varepsilon_{\Gamma_\gamma}$ provides the elastic constant $C_{\Gamma_\gamma}(T)$ described as

$$C_{\Gamma_\gamma}(T) = C_{\Gamma_\gamma}^0 + \sum_{s,k} \frac{\partial^2 E_k^s}{\partial \varepsilon_{\Gamma_\gamma}^2} f_k^s - \frac{1}{k_B T} \sum_{s,k} \left(\frac{\partial E_k^s}{\partial \varepsilon_{\Gamma_\gamma}} \right)^2 f_k^s (1 - f_k^s) + \frac{1}{k_B T} \frac{\sum_{s,k} \left[\frac{\partial E_k^s}{\partial \varepsilon_{\Gamma_\gamma}} f_k^s (1 - f_k^s) \right]^2}{\sum_{s,k} f_k^s (1 - f_k^s)}. \quad (8)$$

Here $f_k^s = \{1 + \exp[(E_{0,k}^s - E_F)/k_B T]\}^{-1}$ is the Fermi distribution function. $\partial E_k^s(\varepsilon_{\Gamma_\gamma})/\partial \varepsilon_{\Gamma_\gamma}|_{\varepsilon_{\Gamma_\gamma} \rightarrow 0}$ and $\partial^2 E_k^s(\varepsilon_{\Gamma_\gamma})/\partial \varepsilon_{\Gamma_\gamma}^2|_{\varepsilon_{\Gamma_\gamma} \rightarrow 0}$ are written as $\partial E_k^s/\partial \varepsilon_{\Gamma_\gamma}$ and $\partial^2 E_k^s/\partial \varepsilon_{\Gamma_\gamma}^2$, respectively. The conservation law for the total electron number with respect to the strain $\partial n/\partial \varepsilon_{\Gamma_\gamma} = \sum_k \partial f_k/\partial \varepsilon_{\Gamma_\gamma} = 0$ is employed to calculate Eq. (8). The second term on the right-hand side of Eq. (8) corresponds to van Vleck term, which originates from the off-diagonal element h_{k,Γ_γ} in the multipole-strain interaction of Eq. (3). The third and fourth terms are the Curie terms ($\sim 1/T$) related to the diagonal elements d_{k,Γ_γ}^l and d_{k,Γ_γ}^u . In this two-band model, the matrix elements of a multipole and the band gap are independent of the wave vector k . The temperature dependence of the elastic constant is obtained

by replacing the sum over the wave vector \sum_k by the energy integral using the DOS of the two-band model shown in Fig. 6 as [35]

$$C_{\Gamma_\gamma}(T) = C_{\Gamma_\gamma}^0 - \frac{1}{4}D(d_{\Gamma_\gamma}^u - d_{\Gamma_\gamma}^l)^2 \times \left[\tanh \left(\frac{\Delta + W}{2k_B T} \right) - \tanh \left(\frac{\Delta}{2k_B T} \right) \right] + D|h_{\Gamma_\gamma}|^2 \frac{2k_B T}{\Delta} \ln \left| \frac{\cosh \left(\frac{\Delta}{2k_B T} \right)}{\cosh \left(\frac{\Delta + W}{2k_B T} \right)} \right|. \quad (9)$$

Here we adopt the background elastic constant $C_{\Gamma_\gamma}^0 = A - B/(e^{C/T} - 1)$ [30]. $C_{\Gamma_\gamma}^0$, $D(d_{\Gamma_\gamma}^u - d_{\Gamma_\gamma}^l)^2$, and $D|h_{\Gamma_\gamma}|^2$ in Eq. (9) are treated as fit parameters. The second and third terms in Eq. (9) correspond to Curie and van Vleck term, respectively.

The analysis by the multipole susceptibility of Eq. (9) reveals the contribution of valence fluctuations to the elastic constant in zero field. Fits to the temperature dependence of the elastic constants C_{44} , C_T , and C_B in zero field are shown in Fig. 2. The fit parameters are summarized in Table II. Here we adopt $\Delta = 70$ K and $W = 55$ K at 0 T as determined by the analysis of specific-heat data of YbB_{12} based on the rectangular two-band model [7]. The temperature dependence of the elastic constants C_{44} , C_T , and C_B can be well described by our model. The energy gap Δ , the bandwidth W , and the coefficient of the Curie term $D(d_{\Gamma_\gamma}^u - d_{\Gamma_\gamma}^l)^2$, are necessary to reproduce the additional contribution in the vicinity of $T^* = 35$ K. In contrast, the van Vleck contribution is not needed to explain the experimental results. Our results indicate the importance of the multipole-strain interaction [Eq. (3)] to the elastic constants. In particular, the broad increase of C_B below ~ 40 K seems to be the result of the isotropic change of the ionic radii caused by valence fluctuations due to the c - f hybridization. We also tried to fit C_B to adopt $\Delta = 30$ K as determined by the high-field magnetoresistance [11]. However, we are not able to reproduce the curvature change in C_B around 35 K (see Appendix D).

The multipole susceptibility also provides the renormalized multipole-strain coupling constant and the interaction anisotropy. For the volume strain ε_B , the first-order coefficient of the energy gap is described as $d\Delta(\varepsilon_B)/d\varepsilon_B|_{\varepsilon_B \rightarrow 0} = (d_B^u - d_B^l)/2$ from Eq. (6). We can change the variable of this relation from ε_B to the hydrostatic pressure P , because $P = C_B \varepsilon_B$. In addition, we assume that Δ_k in Eq. (6) corresponds to the activation energy E determined by resistivity

measurements. Thus, based on the hydrostatic pressure dependence of the resistivity of YbB_{12} [36], we can estimate the renormalized hexadecapole-strain coupling constant $|d_B^u - d_B^l|/k_B$ to be 326 K by $dE/dP = -0.809 \text{ K/GPa} = -8.09 \times 10^{-10} \text{ K/(J/m}^3\text{)}$ for $C_B = 20.146 \times 10^{10} \text{ J/m}^3$ (Table II). This assumption also provides the DOS in zero field to be $D = 2.25 \times 10^{27} \text{ K}^{-1} \text{ m}^{-3}$ from $D(d_B^u - d_B^l)^2 = 3.30 \times 10^9 \text{ J/m}^3$ in Table II. Accordingly, the coupling constant for each elastic mode was calculated (Table II). The coupling constant for C_{44} is approximately 5 and 3 times smaller than the coupling constant for C_T and C_B , respectively. Therefore, the dominant interaction is caused by the bulk strain with Γ_1 and the symmetry-breaking strain with Γ_3 . This result is useful to elucidate the quantum states, which carry the multipole degrees of freedom.

While valence fluctuations are caused by hexadecapole-strain interactions in YbB_{12} , the contribution of the fluctuations to the elasticity is unexpectedly small in zero field. As shown in Fig. 2, C_B does not exhibit a softening in YbB_{12} . This result is quite different from the 3.8% softening in C_B observed for SmB_6 . Furthermore, the coupling constant $|d_B^u - d_B^l|/k_B = 326 \text{ K}$ of YbB_{12} is approximately 4 times smaller than 1280 K reported for C_B of SmB_6 [23].

In contrast to zero field, strong valence fluctuations are revealed in applied magnetic fields. A fit to the temperature-dependent data of C_B at 58 T is shown in Fig. 5 (dashed line). The fit parameters at 58 T are also summarized in Table II. In this analysis we did not change C_B^0 from that in zero field. We fixed the bandwidth $W = 55 \text{ K}$ as the previously proposed rigid-band model [15]. The softening with the minimum at 40 K is reproduced qualitatively. Notably, the coefficient of the Curie term $D(d_B^u - d_B^l)^2$ is enhanced from $3.30 \times 10^9 \text{ J/m}^3$ at 0 T to $10.3 \times 10^9 \text{ J/m}^3$ at 58 T. Thus, the quantum state contributing to the Curie term of YbB_{12} might approach that of SmB_6 in magnetic fields. We stress that the hexadecapole-strain interaction originates from the coupling between the isotropic volume change of the crystal lattice and the change of ionic radii due to valence fluctuations. Therefore, the larger $D(d_B^u - d_B^l)^2$ in magnetic fields indicates the enhancement of valence fluctuations of Yb.

A reduced energy gap is a plausible result of the IM transition. Our analysis reveals that the energy gap $2\Delta = 140 \text{ K}$ at 0 T is reduced to 74 K at 58 T. This may be attributed to the Zeeman effect that changes the energy of the $4f$ states (see Appendix C). However, this two-band model cannot describe the gap closing in high fields. Since the DOS is approximated as constant, we cannot describe the IM transition due to the overlap of the edge of DOS at the Fermi energy as schematically illustrated in Fig. 6. An analysis using more realistic DOS as proposed in a previous study [10,15] is needed to describe the field-induced metal state in high fields.

Since the DOS in zero field is estimated by using the pressure dependence of the activation energy of YbB_{12} , we cannot apply D to estimate the coupling constant $|d_B^u - d_B^l|/k_B$ in high fields. Nevertheless, if we estimate the coupling constant assuming a field-independent rigid-band model with energy gap, the field-enhanced value of 576 K can be obtained. The increase in the elastic softening due to the increase in the coupling constant is also consistent with a previous

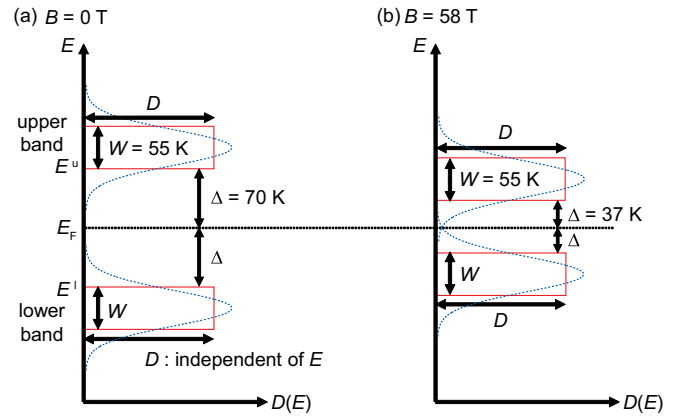


FIG. 6. Schematic view of the two-band model assuming a constant DOS over each band (red rectangular). (a) DOS at zero field with an energy gap $2\Delta = 140 \text{ K}$ and bandwidth $W = 55 \text{ K}$. (b) DOS at 58 T. The energy gap $2\Delta = 74 \text{ K}$ and the bandwidth $W = 55 \text{ K}$ is determined using Eq. (9). The blue dotted curves indicate the schematic view of a more realistic DOS of YbB_{12} .

theoretical study of the electron-phonon coupling mediated by conduction electrons and f electrons [27]. Although the model needs to be improved, this interpretation seems to be plausible.

For further discussion of the field-enhanced valence fluctuations in YbB_{12} , we estimated the valence change of Yb in high fields. Previous studies on SmB_6 have revealed a valence change from 2.59 ± 0.01 at 300 K to 2.53 ± 0.01 at 60 K [37] and a softening of C_B by 3.1% from 300 to 60 K [23]. We assume that the valence change is proportional to the amount of elastic softening as a result of hexadecapole-strain interaction. Thus, the valence change is estimated to be -0.019 per 1% of elastic softening. Since the softening of C_B in SmB_6 and YbB_{12} are described by the hexadecapole susceptibility based on the two-band model, we assume that the valence change per elastic softening applies to YbB_{12} as well. Since the contribution of the hexadecapole-strain interaction to the elastic softening in YbB_{12} , namely the coefficient of the Curie term $D(d_B^u - d_B^l)^2$, is 2.5 times smaller than in SmB_6 (Table II), the contribution of valence fluctuations to the elastic softening in YbB_{12} is reduced by a factor of 2.5. At 1.4 K, in the high-field Kondo-metal phase, the 0.09% softening from B_{IM} to 58 T (Fig. 3) indicates a small valence change of only approximately -0.00069 . Furthermore, at 40 K, a valence change of approximately -0.0040 is estimated from the 0.52% softening of C_B . Such a valence change at 40 K may be detectable by high-field synchrotron x-ray measurements [38].

Our results seem to be in conflict with the localized tendency of $4f$ states in the magnetic fields [39–41]. For a comprehensive understanding of the results, we discuss the Zeeman mixing and hybridization between Yb and B electrons in addition to the c - f hybridization due to the $5d$ and $4f$ electrons of the Yb atoms. In YbB_{12} , the contribution of the Γ_6 and Γ_7 states to the ground state is enhanced by the Zeeman effect (see Appendix C, Fig. 9). Thus, we expect that magnetic fields reduce the anisotropy of the electronic states due to the contributions of the Γ_8 , Γ_6 , and Γ_7 wave functions

in YbB₁₂. In addition, as shown in Fig. 1(a), the Yb ion of YbB₁₂ is surrounded by a highly isotropic cage made up of 24 borons. This indicates an isotropic hybridization between the Yb 4*f* electrons and the B 2*p* electrons in addition to the 5*d*-4*f* hybridization. Thus, we suggest that the valence fluctuations are induced by the interatomic *p*-*f* hybridization due to the isotropic wave function in high fields. Furthermore, a field-induced *p*-*f* hybridization is consistent with the enhancement of the hexadecapole-strain interaction in high fields. In general, the matrix element of the hexadecapole H_0 for the wave function ψ is given by $\int d\mathbf{r} \psi^* H_0 \psi$. Therefore, a spatially expanded wave function, which is expected due to the interatomic type *p*-*f* hybridization, might enhance the renormalized multipole-strain coupling $d_B^{u(1)}$ in Eq. (3). Our assumption is consistent with the isotropic resistivity in the low-temperature Kondo-metal phase [14]. Although the crystal structure and magnetic character are different from those of YbB₁₂, the similar mechanisms of field-induced *p*-*f* hybridization and delocalization of 4*f* electrons have been proposed in the heavy-fermion compound CeRhIn₅ to describe the emergence of an anisotropic electronic state in high fields [42–45].

V. CONCLUSION

In the present work we investigated valence fluctuations of YbB₁₂ in zero and high fields by use of ultrasonic measurements. In zero field, the additional elastic hardening of C_{11} , C_{44} , $C_T = (C_{11} - C_{12})/2$, and the bulk modulus $C_B = (C_{11} + 2C_{12})/3$ indicates only a small contribution of valence fluctuations to the elastic constants. In the Kondo-metal state, the valence fluctuations due to the *c*-*f* hybridization are suggested to be enhanced by the field-induced elastic softening of C_B . We found signatures of strong field-induced valence fluctuations in the vicinity of 40 K. Our phenomenological analysis of the temperature dependence of C_B based on the two-band model reveals that both the additional contribution in zero field and the field-induced elastic softening are reasonably described by the hexadecapole susceptibility. In particular, the field-induced elastic softening is attributed to the enhancement of the hexadecapole-strain coupling. This result indicates that the magnetic field enhances an isotropic volume change of the crystal lattice and the change of ionic radii due to valence fluctuations. Therefore, we propose field-induced valence fluctuations due to *c*-*f* hybridization in YbB₁₂. In particular, we propose that the *p*-*f* hybridization between Yb-4*f* and B-2*p* electrons plays a key role in high fields. The observed decrease of the energy gap in magnetic fields is explained by the energy shift of the 4*f* electrons due to the Zeeman effect.

Our study shows that ultrasonic measurements are useful to detect valence fluctuations. As suggested by a theoretical work [46], such measurements may play a key role in the study of valence quantum criticality. We expect that field-induced valence fluctuations appear in other valence-fluctuating compounds.

ACKNOWLEDGMENTS

The authors thank Yuichi Nemoto and Mitsuhiro Akatsu for supplying the LiNbO₃ piezoelectric transducers. We also thank Keisuke Mitsumoto and Shintaro Nakamura for

valuable discussions. This work was partly supported by JSPS Bilateral Joint Research Projects (JPJSBP120193507) and Grants-in-Aid for young scientists (KAKENHI JP20K14404) and scientific research (KAKENHI JP20K03854). We acknowledge the support of the HLD at HZDR, member of the European Magnetic Field Laboratory (EMFL), the Deutsche Forschungsgemeinschaft (DFG) through the Würzburg-Dresden Cluster of Excellence on Complexity and Topology in Quantum Matter - *ct.qmat* (EXC 2147, project No. 390858490), and the BMBF via DAAD (project No 57457940).

APPENDIX A: TEMPERATURE DEPENDENCE OF ELASTIC CONSTANT C_{11}

Figure 7 shows the temperature dependence of the elastic constant C_{11} in a wide temperature range of up to 300 K. C_{11} exhibits an increase with decreasing temperatures from 300 K. This result indicates the elastic hardening of the bulk modulus C_B from 300 K down to low temperatures.

APPENDIX B: MULTIPOLE SUSCEPTIBILITY FOR CEF WAVE FUNCTIONS IN ZERO FIELD

Here we present the CEF wave functions, the multipole matrices, and multipole susceptibility of YbB₁₂ assuming the localized 4*f* electrons. We show that the multipole susceptibility cannot describe our experimental results in Fig. 2.

To calculate the multipole susceptibility of YbB₁₂, we use CEF wave functions of the 4*f* electrons for Yb³⁺ with the total angular momentum $J = 7/2$. The CEF Hamiltonian H_{CEF} under O_h symmetry is written as

$$H_{\text{CEF}} = B_4(O_4^0 + 5O_4^4) + B_6(O_6^0 - 21O_6^4). \quad (\text{B1})$$

Here B_4 and B_6 are the CEF parameters. The matrix elements of O_4^0 , O_4^4 , O_6^0 , and O_6^4 for $|J_z\rangle$ are listed in Ref. [47]. The wave functions diagonalizing H_{CEF} are given by [4]

$$|\Gamma_8^{1\pm}\rangle = -\sqrt{\frac{7}{12}} \left| \pm \frac{7}{2} \right\rangle + \sqrt{\frac{5}{12}} \left| \mp \frac{1}{2} \right\rangle, \quad (\text{B2})$$

$$|\Gamma_8^{2\pm}\rangle = \frac{1}{2} \left| \pm \frac{5}{2} \right\rangle + \frac{\sqrt{3}}{2} \left| \mp \frac{3}{2} \right\rangle, \quad (\text{B3})$$

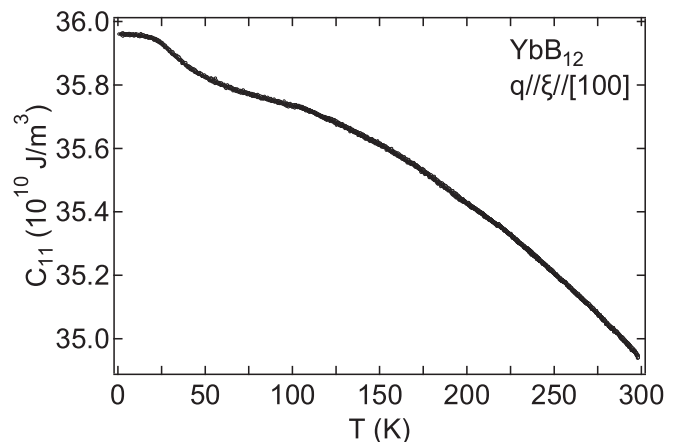


FIG. 7. Temperature dependence of the longitudinal elastic constant C_{11} .

$$|\Gamma_6^{1\pm}\rangle = \sqrt{\frac{5}{12}}|\pm\frac{7}{2}\rangle + \sqrt{\frac{7}{12}}|\mp\frac{1}{2}\rangle, \quad (\text{B4})$$

$$|\Gamma_7^\pm\rangle = -\frac{\sqrt{3}}{2}\left|\pm\frac{5}{2}\right\rangle + \frac{1}{2}\left|\mp\frac{3}{2}\right\rangle, \quad (\text{B5})$$

where $|\Gamma_8^{1\pm}\rangle$ and $|\Gamma_8^{2\pm}\rangle$ are the ground-state wave functions and $|\Gamma_7^\pm\rangle$ and $|\Gamma_6^\pm\rangle$ are the degenerate excited states. The matrix elements of H_{CEF} for the wave func-

tions given in Eqs. (B2)–(B5) provide the eigenenergy of each CEF state described as $E_{\Gamma_8} = 120(B_4 + 168B_6)$, $E_{\Gamma_6} = 120(7B_4 - 210B_6)$, and $E_{\Gamma_7} = -120(9B_4 + 126B_6)$. The energy gap $\Delta_{\text{CEF}} = 23 \text{ meV} = 270 \text{ K}$ between the ground state and the excited states Γ_6 and Γ_7 [4] provides the CEF parameters $B_4 = -33.7 \text{ meV}$ and $B_6 = -6.24 \text{ meV}$.

The matrices of the hexadecapole $H_0 = O_4^0 + 5O_4^4$ with irrep Γ_1 , the quadrupoles O_u and O_v with Γ_3 , and O_{yz} , O_{zx} , and O_{xy} with Γ_5 for the wave functions (B2)–(B5) are calculated as

$$H_0 = \begin{pmatrix} |\Gamma_8^{1+}\rangle & |\Gamma_8^{1-}\rangle & |\Gamma_8^{2+}\rangle & |\Gamma_8^{2-}\rangle & |\Gamma_6^+\rangle & |\Gamma_6^-\rangle & |\Gamma_7^+\rangle & |\Gamma_7^-\rangle \\ 120 & 0 & 0 & 0 & 0 & 0 & 0 & 0 \\ 0 & 120 & 0 & 0 & 0 & 0 & 0 & 0 \\ 0 & 0 & 120 & 0 & 0 & 0 & 0 & 0 \\ 0 & 0 & 0 & 120 & 0 & 0 & 0 & 0 \\ 0 & 0 & 0 & 0 & 840 & 0 & 0 & 0 \\ 0 & 0 & 0 & 0 & 0 & 840 & 0 & 0 \\ 0 & 0 & 0 & 0 & 0 & 0 & 1080 & 0 \\ 0 & 0 & 0 & 0 & 0 & 0 & 0 & 1080 \end{pmatrix}, \quad (\text{B6})$$

$$O_u = \begin{pmatrix} 6 & 0 & 0 & 0 & -3\sqrt{35} & 0 & 0 & 0 \\ 0 & 6 & 0 & 0 & 0 & -3\sqrt{35} & 0 & 0 \\ 0 & 0 & -6 & 0 & 0 & 0 & -3\sqrt{3} & 0 \\ 0 & 0 & 0 & -6 & 0 & 0 & 0 & -3\sqrt{3} \\ -3\sqrt{35} & 0 & 0 & 0 & 0 & 0 & 0 & 0 \\ 0 & -3\sqrt{35} & 0 & 0 & 0 & 0 & 0 & 0 \\ 0 & 0 & -3\sqrt{3} & 0 & 0 & 0 & 0 & 0 \\ 0 & 0 & 0 & -3\sqrt{3} & 0 & 0 & 0 & 0 \end{pmatrix}, \quad (\text{B7})$$

$$O_v = \begin{pmatrix} 0 & 0 & 0 & \sqrt{105} & 0 & 0 & 0 & 0 \\ 0 & 0 & 2\sqrt{3} & 0 & 0 & 0 & -3 & 0 \\ 0 & 2\sqrt{3} & 0 & 0 & 0 & \sqrt{105} & 0 & 0 \\ \sqrt{105} & 0 & 0 & 0 & 2\sqrt{3} & 0 & 0 & 0 \\ 0 & 0 & 0 & 2\sqrt{3} & 0 & 0 & 0 & -3 \\ 0 & 0 & \sqrt{105} & 0 & 0 & 0 & 0 & 0 \\ 0 & -3 & 0 & 0 & 0 & 0 & 0 & 0 \\ 0 & 0 & 0 & 0 & -3 & 0 & 0 & 0 \end{pmatrix}, \quad (\text{B8})$$

$$O_{yz} = \begin{pmatrix} 0 & 0 & 0 & 0 & 0 & 0 & \sqrt{35}i & 0 \\ 0 & 0 & 0 & 3\sqrt{3}i & 0 & 0 & 0 & -4i \\ 0 & 0 & 0 & 0 & -3\sqrt{3}i & 0 & 0 & -2\sqrt{3}i \\ 0 & -3\sqrt{3}i & 0 & 0 & 0 & 0 & -2\sqrt{3}i & 0 \\ 0 & 0 & 3\sqrt{3}i & 0 & 0 & 0 & -4i & 0 \\ 0 & 0 & 0 & 0 & 0 & 0 & 0 & \sqrt{35}i \\ -\sqrt{35}i & 0 & 0 & 2\sqrt{3}i & 4i & 0 & 0 & 0 \\ 0 & 4i & 2\sqrt{3}i & 0 & 0 & -\sqrt{35}i & 0 & 0 \end{pmatrix}, \quad (\text{B9})$$

$$O_{zx} = \begin{pmatrix} 0 & 0 & 0 & 0 & 0 & 0 & -\sqrt{35} & 0 \\ 0 & 0 & 0 & 3\sqrt{3} & 0 & 0 & 0 & -4 \\ 0 & 0 & 0 & 0 & -3\sqrt{3} & 0 & 0 & 4\sqrt{3} \\ 0 & 3\sqrt{3} & 0 & 0 & 0 & 0 & -4\sqrt{3} & 0 \\ 0 & 0 & -3\sqrt{3} & 0 & 0 & 0 & 4 & 0 \\ 0 & 0 & 0 & 0 & 0 & 0 & 0 & \sqrt{35} \\ -\sqrt{35} & 0 & 0 & -4\sqrt{3} & 4 & 0 & 0 & 0 \\ 0 & -4 & 4\sqrt{3} & 0 & 0 & \sqrt{35} & 0 & 0 \end{pmatrix}, \quad (\text{B10})$$

$$O_{xy} = \begin{pmatrix} 0 & 0 & 0 & 0 & 0 & 0 & 0 & -\sqrt{35}i \\ 0 & 0 & 3\sqrt{3}i & 0 & 0 & 0 & 8i & 0 \\ 0 & -3\sqrt{3}i & 0 & 0 & 0 & 0 & 0 & 0 \\ 0 & 0 & 0 & 0 & 3\sqrt{3}i & 0 & 0 & 0 \\ 0 & 0 & 0 & -3\sqrt{3}i & 0 & 0 & 0 & -8i \\ 0 & 0 & 0 & 0 & 0 & 0 & \sqrt{35}i & 0 \\ 0 & -8i & 0 & 0 & 0 & -\sqrt{35}i & 0 & 0 \\ \sqrt{35}i & 0 & 0 & 0 & 8i & 0 & 0 & 0 \end{pmatrix}. \quad (\text{B11})$$

Here Stevens equivalent operators $O_u = 3J_z^2 - J(J+1)$, $O_v = J_x^2 - J_y^2$, $O_{yz} = J_y J_z + J_z J_y$, $O_{zx} = J_z J_x + J_x J_z$, and $O_{xy} = J_x J_y + J_y J_x$, given by the components of the total angular momentum J_x , J_y , and J_z , are used to calculate the matrix elements. Considering the second-order perturbation processes for the i th CEF state with energy E_i^0 due to the multipole-strain interaction of Eq. (2), which is described as

$$E_i(\varepsilon_{\Gamma_\gamma}) = E_i^0 - g_{\Gamma_\gamma} \langle i | O_{\Gamma_\gamma} | i \rangle \varepsilon_{\Gamma_\gamma} - g_{\Gamma_\gamma}^2 \sum_{j \neq i} \frac{|\langle i | O_{\Gamma_\gamma} | j \rangle|^2}{E_j^0 - E_i^0} \varepsilon_{\Gamma_\gamma}^2, \quad (\text{B12})$$

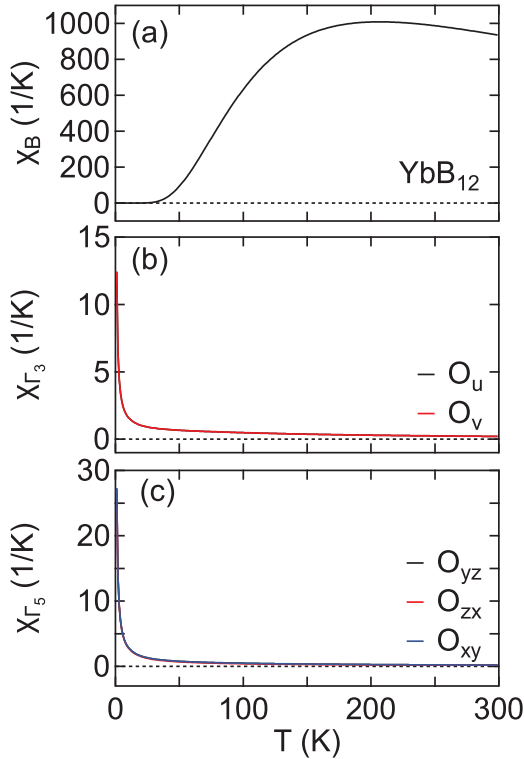


FIG. 8. Temperature dependence of the electric multipole susceptibility of YbB_{12} . (a) Hexadecapole susceptibility χ_B of $H_0 = O_4^0 + 5O_4^4$ with Γ_1 . This susceptibility provides the temperature dependence of the bulk modulus C_B . (b) Quadrupole susceptibility χ_{Γ_3} of O_u and O_v with Γ_3 related to $(C_{11} - C_{12})/2$. (c) Quadrupole susceptibility χ_{Γ_5} of O_{yz} , O_{zx} , and O_{xy} with Γ_5 related to C_{44} . As indicated in Eq. (B14), $-\chi_{\Gamma_\gamma}$ contributes to these elastic constants. (The curves for O_u and O_v as well as for O_{yz} , O_{zx} , and O_{xy} virtually lie on top of each other.)

the total free energy F , which consists of the CEF state and the strain, is written as

$$F(T, \varepsilon_{\Gamma_\gamma}) = \frac{1}{2} C_{\Gamma_\gamma}^0 \varepsilon_{\Gamma_\gamma}^2 - N k_B T \ln Z(\varepsilon_{\Gamma_\gamma}). \quad (\text{B13})$$

Here N is the number of Yb ions per unit volume and $Z(\varepsilon_{\Gamma_\gamma})$ is the partition function written as $Z(\varepsilon_{\Gamma_\gamma}) = \sum_i \exp[-E_i(\varepsilon_{\Gamma_\gamma})/k_B T]$. Thus, the elastic constant and the multipole susceptibility are calculated as

$$C_{\Gamma_\gamma} = \frac{\partial^2 F}{\partial \varepsilon_{\Gamma_\gamma}^2} = C_{\Gamma_\gamma}^0 - N g_{\Gamma_\gamma}^2 \chi_{\Gamma_\gamma}, \quad (\text{B14})$$

$$-g_{\Gamma_\gamma}^2 \chi_{\Gamma_\gamma} = \left\langle \frac{\partial^2 E}{\partial \varepsilon_{\Gamma_\gamma}^2} \right\rangle - \frac{1}{k_B T} \left\{ \left\langle \left(\frac{\partial E}{\partial \varepsilon_{\Gamma_\gamma}} \right)^2 \right\rangle - \left\langle \frac{\partial E}{\partial \varepsilon_{\Gamma_\gamma}} \right\rangle^2 \right\}. \quad (\text{B15})$$

Here $C_{\Gamma_\gamma}^0$ is a background elastic constant, $\langle A \rangle$ is the thermal average using Boltzmann statistics written as $\langle A \rangle = \sum_i A_i \exp[-E_i/k_B T]/Z$, and $\partial E(\varepsilon_{\Gamma_\gamma})/\partial \varepsilon_{\Gamma_\gamma}|_{\varepsilon_{\Gamma_\gamma} \rightarrow 0}$

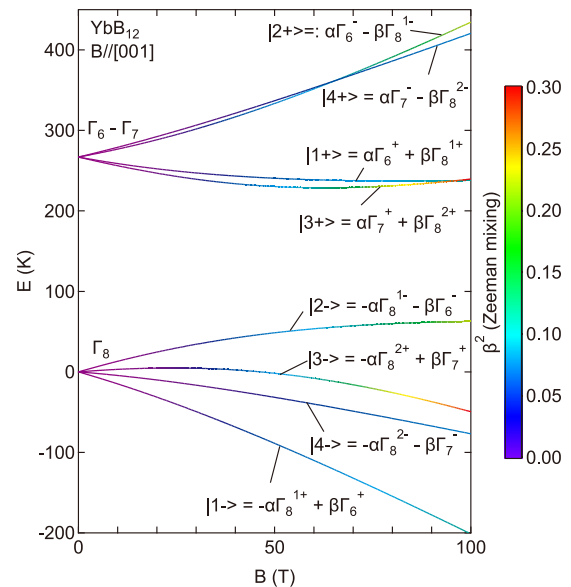


FIG. 9. Magnetic-field dependence of the eigenenergy in H_{total} of Eq. (C3) for $B \parallel [001]$. The color code shows the Zeeman mixing ratio β^2 in the wave functions of Eqs. (C16)–(C23).

and $\partial^2 E(\varepsilon_{\Gamma_\gamma})/\partial \varepsilon_{\Gamma_\gamma}^2|_{\varepsilon_{\Gamma_\gamma} \rightarrow 0}$ are written as $\partial E/\partial \varepsilon_{\Gamma_\gamma}$ and $\partial^2 E/\partial \varepsilon_{\Gamma_\gamma}^2$, respectively. The first term on the right-hand side of Eq. (B15) corresponds to van Vleck term being constant at low temperatures and the second one to Curie term showing the reciprocal temperature dependence. The calculated multipole susceptibility χ_{Γ_γ} is shown in Fig. 8.

The hexadecapole susceptibility χ_B would indicate a monotonic hardening of C_B below 100 K down to low temperatures because the temperature dependence of the elastic constant C_{Γ_γ} is given by $-\chi_B$, i.e., the second term in Eq. (B14). The divergent behavior of χ_{Γ_3} and χ_{Γ_5} would predict an elastic softening of $(C_{11} - C_{12})/2$ and C_{44} at low temperatures, respectively. However, our experimental results of YbB₁₂ in zero field cannot be described by the susceptibility based on CEF wave functions using this picture, i.e., localized 4*f* electrons.

APPENDIX C: HEXADECAPOLE SUSCEPTIBILITY FOR CEF WAVE FUNCTIONS IN MAGNETIC FIELDS

In this Appendix the CEF wave functions, the hexadecapole matrix, and the hexadecapole susceptibility in magnetic fields of YbB₁₂ are presented assuming localized 4*f* electrons. We show that the elastic softening of C_B in high fields cannot be described by the hexadecapole susceptibility χ_B .

To calculate the hexadecapole susceptibility in magnetic fields, we consider the Zeeman Hamiltonian for $B \parallel [001]$ given by

$$H_{\text{Zeeman}} = -g_J \mu_B B_0 J_z. \quad (\text{C1})$$

Here g_J is the Landé g factor, μ_B is the Bohr magneton, B_0 is the magnetic field, and J_z is the magnetic dipole. Using the CEF wave functions of Eqs. (B2)–(B5), the matrix of H_{Zeeman} of Eq. (C1) is written as

$$H_{\text{Zeeman}} = \begin{pmatrix} -\frac{11}{6}B & 0 & 0 & 0 & \frac{\sqrt{35}}{3}B & 0 & 0 & 0 \\ 0 & \frac{11}{6}B & 0 & 0 & 0 & -\frac{\sqrt{35}}{3}B & 0 & 0 \\ 0 & 0 & \frac{1}{2}B & 0 & 0 & 0 & \sqrt{3}B & 0 \\ 0 & 0 & 0 & -\frac{1}{2}B & 0 & 0 & 0 & -\sqrt{3}B \\ \frac{\sqrt{35}}{3}B & 0 & 0 & 0 & -\frac{7}{6}B & 0 & 0 & 0 \\ 0 & -\frac{\sqrt{35}}{3}B & 0 & 0 & 0 & \frac{7}{6}B & 0 & 0 \\ 0 & 0 & \sqrt{3}B & 0 & 0 & 0 & -\frac{3}{2}B & 0 \\ 0 & 0 & 0 & -\sqrt{3}B & 0 & 0 & 0 & \frac{3}{2}B \end{pmatrix}. \quad (\text{C2})$$

Here, for the convenience, B in the matrix elements of Eq. (C2) is set as $B = g_J \mu_B B_0$. The total Hamiltonian $H_{\text{total}} = H_{\text{CEF}} + H_{\text{Zeeman}}$ is diagonalized as

$$H_{\text{total}} = \begin{pmatrix} |1+\rangle & |1-\rangle & |2+\rangle & |2-\rangle & |3+\rangle & |3-\rangle & |4+\rangle & |4-\rangle \\ \begin{matrix} E_1^+ & 0 & 0 & 0 & 0 & 0 & 0 & 0 \\ 0 & E_1^- & 0 & 0 & 0 & 0 & 0 & 0 \\ 0 & 0 & E_2^+ & 0 & 0 & 0 & 0 & 0 \\ 0 & 0 & 0 & E_2^- & 0 & 0 & 0 & 0 \\ 0 & 0 & 0 & 0 & E_3^+ & 0 & 0 & 0 \\ 0 & 0 & 0 & 0 & 0 & E_3^- & 0 & 0 \\ 0 & 0 & 0 & 0 & 0 & 0 & E_4^+ & 0 \\ 0 & 0 & 0 & 0 & 0 & 0 & 0 & E_4^- \end{matrix} \end{pmatrix}. \quad (\text{C3})$$

Here the eigenenergies in the matrix of Eq. (C3) are written as

$$E_1^\pm = \frac{\Delta_{\text{CEF}} - 3B}{2} \pm \delta E_1, \quad (\text{C4})$$

$$E_2^\pm = \frac{\Delta_{\text{CEF}} + 3B}{2} \pm \delta E_2, \quad (\text{C5})$$

$$E_3^\pm = \frac{\Delta_{\text{CEF}} - B}{2} \pm \delta E_3, \quad (\text{C6})$$

$$E_4^\pm = \frac{\Delta_{\text{CEF}} + B}{2} \pm \delta E_4. \quad (\text{C7})$$

For convenience, δE_i in Eqs. (C4)–(C7) is set as

$$\delta E_1 = \sqrt{\Delta E_1^2 + \frac{35}{9}B^2}, \quad (\text{C8})$$

$$\delta E_2 = \sqrt{\Delta E_2^2 + \frac{35}{9}B^2}, \quad (\text{C9})$$

$$\delta E_3 = \sqrt{\Delta E_3^2 + 3B^2}, \quad (\text{C10})$$

$$\delta E_4 = \sqrt{\Delta E_4^2 + 3B^2}. \quad (\text{C11})$$

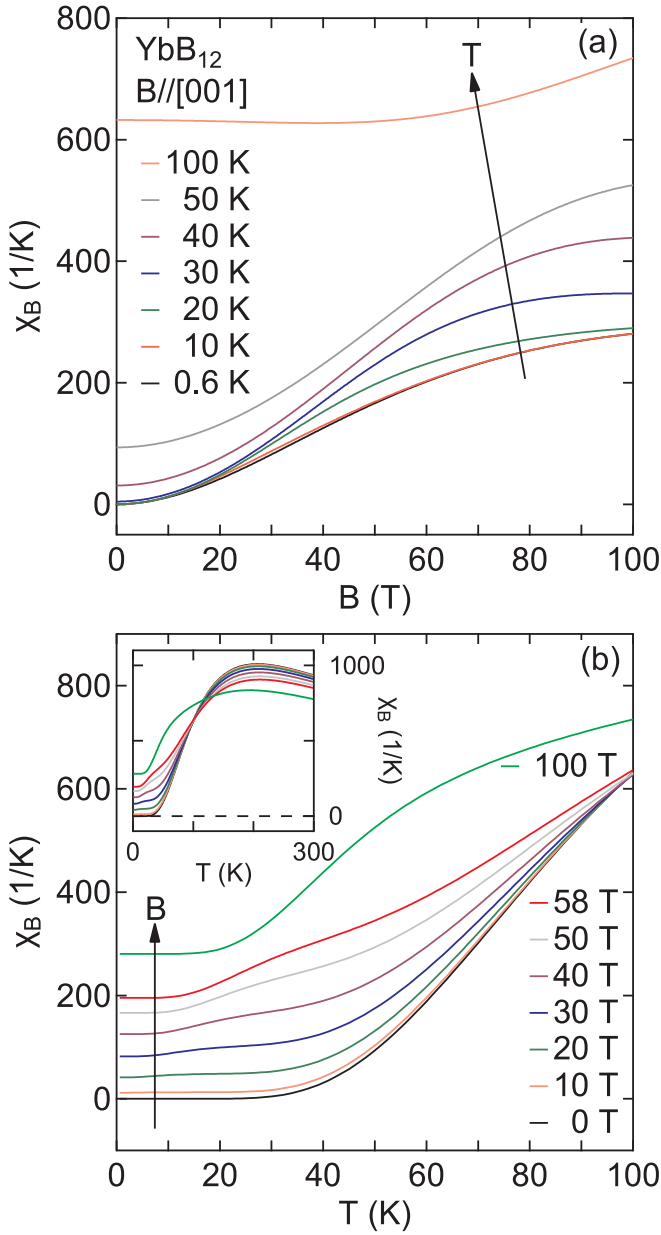


FIG. 10. Electric hexadecapole susceptibility χ_B of YbB_{12} for $B\parallel[001]$. (a) Magnetic-field dependence of χ_B at several temperatures. (b) Temperature dependence of χ_B below 100 K in several magnetic fields. In the inset in (b), χ_B is shown up to 300 K.

We also set ΔE_i in Eqs. (C8)–(C11) as follows:

$$\Delta E_1 = \frac{\Delta_{\text{CEF}}}{2} + \frac{1}{3}B, \quad (\text{C12})$$

$$\Delta E_2 = \frac{\Delta_{\text{CEF}}}{2} - \frac{1}{3}B, \quad (\text{C13})$$

$$\Delta E_3 = \frac{\Delta_{\text{CEF}}}{2} - B, \quad (\text{C14})$$

$$\Delta E_4 = \frac{\Delta_{\text{CEF}}}{2} + B. \quad (\text{C15})$$

The wave functions diagonalizing the matrix Eq. (C3) are written as

$$|1+\rangle = \alpha_1|\Gamma_6^+\rangle + \beta_1|\Gamma_8^+\rangle, \quad (\text{C16})$$

$$|1-\rangle = \beta_1|\Gamma_6^+\rangle - \alpha_1|\Gamma_8^+\rangle, \quad (\text{C17})$$

$$|2+\rangle = \alpha_2|\Gamma_6^-\rangle - \beta_2|\Gamma_8^-\rangle, \quad (\text{C18})$$

$$|2-\rangle = -\beta_2|\Gamma_6^-\rangle - \alpha_2|\Gamma_8^-\rangle, \quad (\text{C19})$$

$$|3+\rangle = \alpha_3|\Gamma_7^+\rangle + \beta_3|\Gamma_8^{2+}\rangle, \quad (\text{C20})$$

$$|3-\rangle = \beta_3|\Gamma_7^+\rangle - \alpha_3|\Gamma_8^{2+}\rangle, \quad (\text{C21})$$

$$|4+\rangle = \alpha_4|\Gamma_7^-\rangle - \beta_4|\Gamma_8^{2-}\rangle, \quad (\text{C22})$$

$$|4-\rangle = -\beta_4|\Gamma_7^-\rangle - \alpha_4|\Gamma_8^{2-}\rangle. \quad (\text{C23})$$

Here the coefficients α_i and β_i for $i = 1, 2, 3, 4$ in each wave function in Eqs. (C16)–(C23) are set as

$$\alpha_1 = \frac{\Delta E_1 + \delta E_1}{\sqrt{(\Delta E_1 + \delta E_1)^2 + \frac{35}{9}B^2}}, \quad (\text{C24})$$

$$\alpha_2 = \frac{\Delta E_2 + \delta E_2}{\sqrt{(\Delta E_2 + \delta E_2)^2 + \frac{35}{9}B^2}}, \quad (\text{C25})$$

$$\alpha_3 = \frac{\Delta E_3 + \delta E_3}{\sqrt{(\Delta E_3 + \delta E_3)^2 + 3B^2}}, \quad (\text{C26})$$

$$\alpha_4 = \frac{\Delta E_4 + \delta E_4}{\sqrt{(\Delta E_4 + \delta E_4)^2 + 3B^2}}, \quad (\text{C27})$$

$$\beta_i = \sqrt{1 - \alpha_i^2}. \quad (\text{C28})$$

The magnetic-field dependence of the eigenenergies E_i^\pm of Eqs. (C4)–(C7) are shown in Fig. 9. This result is consistent with the previous calculation for YbB_{12} [15]. The multipole susceptibility of Eq. (B15) in magnetic field is calculated using the wave functions of Eqs. (C16)–(C23), the energy of Eqs. (C4)–(C7), the multipole matrices of Eqs. (B6)–(B11), the second-order perturbation of Eq. (B12), and the free energy of Eq. (B13).

In particular, we show the field-dependent hexadecapole susceptibility of H_0 in Fig. 10. Here the matrix of the hexadecapole H_0 is written as

$$H_0 = \begin{pmatrix} |1+\rangle & |1-\rangle \\ 120(6\alpha_1^2 + 1) & 720\alpha_1\beta_1 \\ 720\alpha_1\beta_1 & -120(6\alpha_1^2 - 7) \end{pmatrix} \oplus \begin{pmatrix} |2+\rangle & |2-\rangle \\ 120(6\alpha_2^2 + 1) & -720\alpha_2\beta_2 \\ -720\alpha_2\beta_2 & -120(6\alpha_2^2 - 7) \end{pmatrix} \oplus \begin{pmatrix} |3+\rangle & |3-\rangle \\ -120(10\alpha_3^2 - 1) & -1200\alpha_3\beta_3 \\ -1200\alpha_3\beta_3 & 120(10\alpha_3^2 - 9) \end{pmatrix} \oplus \begin{pmatrix} |4+\rangle & |4-\rangle \\ -120(10\alpha_4^2 - 1) & -1200\alpha_4\beta_4 \\ -1200\alpha_4\beta_4 & 120(10\alpha_4^2 - 9) \end{pmatrix}. \quad (\text{C29})$$

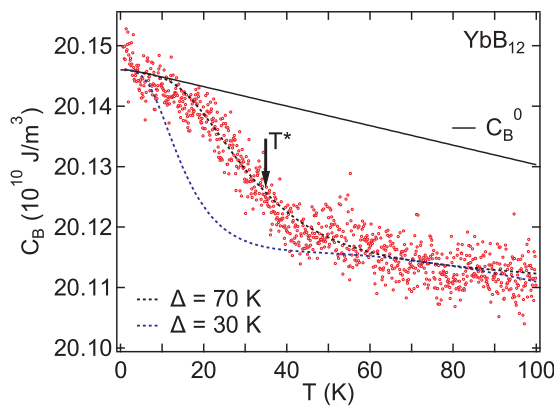


FIG. 11. Fit of the bulk modulus C_B of YbB_{12} by the hexadecapole susceptibility with energy gaps $\Delta = 70$ and 30 K.

The experimental results of the magnetic-field dependence of C_B at 20 , 40 , and 50 K (Fig. 3) can be qualitatively reproduced

by the hexadecapole susceptibility χ_B shown in Fig. 10(a). However, the experimental results of the elastic softening of C_B in high fields (Fig. 5) cannot be described by χ_B shown in Fig. 10(b) since χ_B indicates a hardening of C_B towards lower temperatures. Therefore, our experimental results of YbB_{12} in high magnetic fields cannot be described by the susceptibility based on CEF wave functions of localized $4f$ electrons.

APPENDIX D: HEXADECAPOLE SUSCEPTIBILITY FOR SMALLER ENERGY GAP

Figure 11 shows the fit of bulk modulus C_B in YbB_{12} by the hexadecapole susceptibility with energy gaps $\Delta = 70$ and 30 K. We cannot describe the curvature change for $\Delta = 30$ K, which corresponds to the activation energy determined by the high-field magnetoresistance [11]. This result indicates that the contribution of the larger gap to the elasticity is dominant in zero field in YbB_{12} .

- [1] M. Kasaya, F. Iga, K. Negishi, S. Nakai, and T. Kasuya, *J. Magn. Magn. Mater.* **31–34**, 437 (1983).
- [2] T. Susaki, A. Sekiyama, K. Kobayashi, T. Mizokawa, A. Fujimori, M. Tsunekawa, T. Muro, T. Matsushita, S. Suga, H. Ishii, T. Hanyu, A. Kimura, H. Namatame, M. Taniguchi, T. Miyahara, F. Iga, M. Kasaya, and H. Harima, *Phys. Rev. Lett.* **77**, 4269 (1996).
- [3] K. S. Nemkovski, J.-M. Mignot, P. A. Alekseev, A. S. Ivanov, E. V. Nefedova, A. V. Rybina, L.-P. Regnault, F. Iga, and T. Takabatake, *Phys. Rev. Lett.* **99**, 137204 (2007).
- [4] Y. Kanai, T. Mori, S. Naimen, K. Yamagami, H. Fujiwara, A. Higashiya, T. Kadono, S. Imada, T. Kiss, A. Tanaka, K. Tamasaku, M. Yabashi, T. Ishikawa, F. Iga, and A. Sekiyama, *J. Phys. Soc. Jpn.* **84**, 073705 (2015).
- [5] K. Ikushima, Y. Kato, M. Takigawa, F. Iga, S. Hiura, and T. Takabatake, *Physica B* **281–282**, 274 (2000).
- [6] M. Kasaya, F. Iga, M. Takigawa, and T. Kasuya, *J. Magn. Magn. Mater.* **47–48**, 429 (1985).
- [7] F. Iga, N. Shimizu, and T. Takabatake, *J. Magn. Magn. Mater.* **177–181**, 337 (1998).
- [8] J. Yamaguchi, A. Sekiyama, S. Imada, H. Fujiwara, M. Yano, T. Miyamachi, G. Funabashi, M. Obara, A. Higashiya, K. Tamasaku, M. Yabashi, T. Ishikawa, F. Iga, T. Takabatake, and S. Suga, *Phys. Rev. B* **79**, 125121 (2009).
- [9] T. Saso and H. Harima, *J. Phys. Soc. Jpn.* **72**, 1131 (2003).
- [10] T. Ohashi, A. Koga, S. I. Suga, and N. Kawakami, *Phys. Rev. B* **70**, 245104 (2004).
- [11] K. Sugiyama, F. Iga, M. Kasaya, T. Kasuya, and M. Date, *J. Phys. Soc. Jpn.* **57**, 3946 (1988).
- [12] F. Iga, M. Kasaya, and T. Kasuya, *J. Magn. Magn. Mater.* **76–77**, 156 (1988).
- [13] Y. Takeda, M. Arita, M. Higashiguchi, K. Shimada, H. Namatame, M. Taniguchi, F. Iga, and T. Takabatake, *Phys. Rev. B* **73**, 033202 (2006).
- [14] F. Iga, K. Suga, K. Takeda, S. Michimura, K. Murakami, T. Takabatake, and K. Kindo, *J. Phys.: Conf. Ser.* **200**, 012064 (2010).
- [15] T. T. Terashima, A. Ikeda, Y. H. Matsuda, A. Kondo, K. Kindo, and F. Iga, *J. Phys. Soc. Jpn.* **86**, 054710 (2017).
- [16] Y. H. Matsuda, Y. Murata, T. Inami, K. Ohwada, H. Nojiri, K. Ohoyama, N. Katoh, Y. Murakami, F. Iga, T. Takabatake, A. Mitsuda, and H. Wada, *J. Phys.: Conf. Ser.* **51**, 111 (2006).
- [17] T. T. Terashima, Y. H. Matsuda, Y. Kohama, A. Ikeda, A. Kondo, K. Kindo, and F. Iga, *Phys. Rev. Lett.* **120**, 257206 (2018).
- [18] Z. Xiang, Y. Kasahara, T. Asaba, B. Lawson, C. Tinsman, L. Chen, K. Sugimoto, S. Kawaguchi, Y. Sato, G. Li, S. Yao, Y. L. Chen, F. Iga, J. Singleton, Y. Matsuda, and L. Li, *Science* **362**, 65 (2018).
- [19] B. Lüthi, *Physical Acoustics in the Solid State* (Springer, Berlin, 2005).
- [20] A. Tamaki, T. Goto, S. Kunii, T. Suzuki, T. Fujimura, and T. Kasuya, *J. Phys. C: Solid State Phys.* **18**, 5849 (1985).
- [21] Y. Nemoto, T. Goto, A. Ochiai, and T. Suzuki, *Phys. Rev. B* **61**, 12050 (2000).
- [22] T. Goto, Y. Nemoto, A. Ochiai, and T. Suzuki, *Phys. Rev. B* **59**, 269 (1999).
- [23] S. Nakamura, T. Goto, M. Kasaya, and S. Kunii, *J. Phys. Soc. Jpn.* **60**, 4311 (1991).
- [24] B. Lüthi and M. Yoshizawa, *J. Magn. Magn. Mater.* **63–64**, 274 (1987).
- [25] P. Thalmeier, *J. Phys. C: Solid State Phys.* **20**, 4449 (1987).
- [26] J. Keller, R. Bulla, Th. Höhn, and K. W. Becker, *Phys. Rev. B* **41**, 1878 (1990).
- [27] G. C. Rout, M. S. Ojha, and S. N. Behera, *Physica B* **367**, 101 (2005).
- [28] T. K. Fujita, M. Yoshizawa, R. Kamiya, H. Mitamura, T. Sakakibara, K. Kindo, F. Iga, I. Ishii, and T. Suzuki, *J. Phys. Soc. Jpn.* **80**, SA084 (2011).
- [29] T. Inui, Y. Tanabe, and Y. Onodera, *Group Theory and Its Applications in Physics* (Springer, Berlin, 1990).
- [30] Y. P. Varshni, *Phys. Rev. B* **2**, 3952 (1970).

- [31] Y. Kuramoto, H. Kusunose, and A. Kiss, *J. Phys. Soc. Jpn.* **78**, 072001 (2009).
- [32] S. Nakamura, T. Goto, Y. Ishikawa, S. Sakatsume, and M. Kasaya, *J. Phys. Soc. Jpn.* **60**, 2305 (1991).
- [33] R. Kurihara, K. Mitsumoto, M. Akatsu, Y. Nemoto, T. Goto, Y. Kobayashi, and S. Sato, *J. Phys. Soc. Jpn.* **86**, 064706 (2017).
- [34] B. Lüthi, *J. Magn. Magn. Mater.* **52**, 70 (1985).
- [35] S. Nakamura, T. Goto, T. Fujimura, M. Kasaya, and T. Kasuya, *J. Magn. Magn. Mater.* **76–77**, 312 (1988).
- [36] F. Iga, M. Kasaya, H. Suzuki, Y. Okayama, H. Takabatake, and N. Mori, *Physica B* **186**, 419 (1993).
- [37] M. Mizumaki, S. Tsutsui, and F. Iga, *J. Phys.: Conf. Ser.* **176**, 012034 (2009).
- [38] Y. H. Matsuda, T. Nakamura, K. Kuga, and S. Nakatsuji, *J. Korean Phys. Soc.* **62**, 1778 (2013).
- [39] H. Aoki, S. Uji, A. K. Albessard, and Y. Ōnuki, *Phys. Rev. Lett.* **71**, 2110 (1993).
- [40] Y. H. Matsuda, T. Nakamura, J. L. Her, S. Michimura, T. Inami, K. Kindo, and T. Ebihara, *Phys. Rev. B* **86**, 041109(R) (2012).
- [41] Y. H. Matsuda, J.-L. Her, S. Michimura, T. Inami, T. Ebihara, and H. Amitsuka, *JPS Conf. Proc.* **3**, 011044 (2014).
- [42] P. J. W. Moll, B. Zeng, L. Balicas, S. Geleski, F. F. Balakirev, E. D. Bauer, and F. Ronning, *Nat. Commun.* **6**, 6663 (2015).
- [43] F. Ronning, T. Helm, K. R. Shirer, M. D. Bachmann, L. Balicas, M. K. Chan, B. J. Ramshaw, R. D. McDonald, F. F. Balakirev, M. Jaime, E. D. Bauer, and P. J. W. Moll, *Nature (London)* **548**, 313 (2017).
- [44] P. F. S. Rosa, S. M. Thomas, F. F. Balakirev, E. D. Bauer, R. M. Fernandes, J. D. Thompson, F. Ronning, and M. Jaime, *Phys. Rev. Lett.* **122**, 016402 (2019).
- [45] R. Kurihara, A. Miyake, M. Tokunaga, Y. Hirose, and R. Settai, *Phys. Rev. B* **101**, 155125 (2020).
- [46] S. Watanabe, *J. Phys. Soc. Jpn.* **89**, 073702 (2020).
- [47] M. T. Hutchings, *Solid State Phys.* **16**, 227 (1964).